XIII International Conference on Computational Plasticity. Fundamentals and Applications
COMPLAS XIII
E. Oñate, D.R.J. Owen, D. Peric and M. Chiumenti (Eds)

FINITE ELEMENT MODELLING OF SHEAR BANDS IN POROUS MEDIA BY MEANS OF NON-LOCAL VISCOPLASTICITY

MARIA LAZARI, LORENZO SANAVIA AND BERNHARD A. SCHREFLER

Department of Civil, Architectural and Environmental Engineering (ICEA)
University of Padua (UNIPD)
Via F. Marzolo 9, 35131 Padova, Italy
e-mail: maria.lazari@unipd.it, lorenzo.sanavia@unipd.it, bernhard.schrefler@dicea.unipd.it,
web page: http://www.dicea.unipd.it/

Key words: Viscoplasticity, Non-local approach, Shear bands, Porous media.

Abstract. This work presents a consistent numerical approach in the framework of analyzing the localization process in a slope stability problem. An already existing model, embedded in Mechanics of multiphase porous media, is enhanced with local and non-local elasto-viscoplastic constitutive models to obtain regularized numerical solutions. The initiation and the propagation of the shear band are effectively described by means of FEM analysis, regardless of the mesh size adopted. The strain localization process realistically occurs within the shear band failure mode and its size is governed by the internal length variable, which can be directly estimated by experimental approaches.

1 INTRODUCTION

As it is well known, in the context of the numerical simulation of strain localization with standard finite elements, the shear band width strongly depends on the adopted mesh and in particular equals to the size of the element for each mesh refinement. This fact causes loss of objectivity of the computational results and due to the importance of strain localization especially regarding slope stability, there is a need of regularizing the numerical solution to make predictions of practical value. To this end, suitable constitutive models that induces a characteristic length related to the observed shear band width can be found in the literature, e.g. rate-dependent constitutive models [1-4], gradient plasticity models [5]. Alternatively, kinematics has to be enhanced, e.g. with micropolar continuum [6].

The present contribution deals with the elimination of mesh sensitivity problem in strain localization simulation of multiphase geomaterials for geotechnical applications. A non-local model of integral-type is used in conjunction with viscosity as an extension of an already available viscoplastic Drucker-Prager model with non-associated flow rule [7]. This coupling allows for eliminating mesh dependency in strain localization even in case of weakly rate-sensitive materials (i.e. dense sand) for which viscoplasticity is not sufficient to suit numerical requirement of mesh independency [8]. Following the approach proposed in [9], the viscous nucleus is replaced by an average viscous nucleus (non–local counterpart) over the volume of the structure. When the so-called internal length approaches zero, the local viscoplastic model is regained. The model has been implemented in the finite element code Comes-geo [16-20] allowing for non-local extension to more sophisticated yield criteria only by minor modifications. The efficiency of the models in terms of regularized performance is illustrated

using a benchmark numerical example of a slope failure.

The present study is structured as follows: Section 2 includes the mathematical framework, the main assumptions and features of the model for porous media along with a synopsis of the particular characteristics of viscoplasticity and non-local theories. In Section 3 the numerical results coming out from the simulation of a slope failure problem using local and non-local viscoplasticity are presented, followed by the main conclusions in Section 4.

2 MATHEMATICAL AND NUMERICAL MODEL – A GENERAL DESCRIPTION

In the present work we make use of a mathematic model for non-isothermal variably saturated porous media developed within the Hybrid Mixture Theory [10,11] following [12-15]. For the sake of brevity only a general description of the mathematical framework of the model with its basic assumptions will be presented hereafter and more details regarding its numerical implementation, for the interested reader, is refereed to [16,19].

In the framework of realistic description of natural geomaterials it is necessary to proceed from an unsaturated soil based on a multiphase model. Therefore, the variably saturated porous medium, such as a slope, is treated as a multiphase system consisting of a solid skeleton with open pores filled with liquid water and gas. The gas phase is modelled as an ideal gas composed of dry air (non-condensable gas) and water vapour (condensable gas), which are considered as two miscible species. Phase changes of water (evaporation and condensation) as well as heat transfer through conduction and convection are considered. Furthermore, the non-polar solid is deformable, resulting in a coupling of the fluid, the solid and the thermal fields. All fluid phases are in contact with the solid phase. In the partially saturated zones the liquid water is separated from its vapour by a concave meniscus (capillary water). Due to the curvature of this meniscus, the sorption equilibrium equation [12] gives the relationship, $p^c=p^g-p^w$ between the capillary pressure p^c (also known as matrix suction), gas pressure p^g and liquid water pressure p^w.

The mathematical model consists of four kind of balance equations (mass of dry air, mass of water species, enthalpy of the whole medium and equilibrium equation of the multiphase medium), as well as appropriate constitutive equations for fluids and solid phases. The balance equations were developed in geometrically linear framework and are written in this paper at the macroscopic level considering quasi-static loading conditions. The chosen macroscopic primary variables are: gas pressure, capillary pressure, temperature and displacements, correspond to real measurable quantities directly linked to laboratory practice. This is an important aspect when selecting the appropriate constitutive equations.

The governing equations are discretized in space by means of the standard finite element method (Bubnov-Galerkin method), in time by a fully implicit finite difference scheme (backward difference) and are solved by means of Newton-Raphson type procedure. Further particulars and general references on the numerical treatment can be found in [16,19].

In the following, direct notation will be adopted. Boldface letters will denote vector or tensors and lightface italic letters will be used for scalar quantities.

2.1 Equilibrium equation

The equilibrium equation of the mixture in terms of generalized effective Cauchy's stress tensor $\boldsymbol{\sigma}'(\boldsymbol{x}, t)$ [10,21] assumes the form:

$$\mathrm{div}\left(\boldsymbol{\sigma}' - \left[p^g - S_w p^c\right]\mathbf{1}\right) + \rho\mathbf{g} = 0 \tag{1}$$

where $\rho = [1\text{-}n]\rho^s + nS_w\rho^w + nS_g\rho^g$ is the mass density of the overall medium, $n(\boldsymbol{x}, t)$ is the porosity, $S_w(\boldsymbol{x}, t)$ and $S_g(\boldsymbol{x}, t)$ are respectively the water and gas degree of saturation, $\mathbf{g}$ is the gravity acceleration vector and $\mathbf{1}$ is the second order identity tensor. The form of Eq. (1) assumes the solid grain incompressible, which is common in soil mechanics. In order to consider compressible grains, the Biot coefficient should be present in front of the solid pressure (this becomes important when dealing with rock and concrete).

2.2 Mass balance equations

The mass conservation equation for the mixture of solid skeleton, liquid water and its vapour is:

$$\begin{aligned} & n\left[\rho^w - \rho^{gw}\right]\left[\frac{\partial S_w}{\partial t}\right] + \left[\rho^w S_w + \rho^{gw}\left[1 - S_w\right]\right]\mathrm{div}\left(\frac{\partial \mathbf{u}}{\partial t}\right) \\ & + \left[1 - S_w\right] n \frac{\partial \rho^{gw}}{\partial t} - \mathrm{div}\left(\rho^g \frac{M_\alpha M_w}{M_g^2} \boldsymbol{D}_{\mathrm{g}}^{\mathrm{gw}} \mathrm{grad}\left(\frac{p^{gw}}{p^g}\right)\right) \\ & + \mathrm{div}\left(\rho^w \frac{\mathbf{k}^{\mathrm{w}} k^{rw}}{\mu^w}\left[-\mathrm{grad}(p^g) + \mathrm{grad}(p^c) + \rho^w \mathbf{g}\right]\right) \\ & + \mathrm{div}\left(\rho^{gw} \frac{\mathbf{k}^{\mathrm{g}} k^{rg}}{\mu^g}\left[-\mathrm{grad}(p^g) + \rho^g \mathbf{g}\right]\right) - \beta_{swg} \frac{\partial T}{\partial t} = 0 \end{aligned} \tag{2}$$

where $\mathbf{k}^\pi(\boldsymbol{x}, t) = k^\pi(\boldsymbol{x}, t)\mathbf{1}$ is the intrinsic permeability tensor of the porous matrix in π-fluid saturated condition [m^2], which is assumed to be isotropic, $k^{r\pi}(\boldsymbol{x},t)$ is the fluid relative permeability parameter and $\mu^\pi(\boldsymbol{x}, t)$ is the dynamic viscosity of the fluid [Pa·s], with $\pi = w, g$. $\boldsymbol{D}_{\mathrm{g}}^{\mathrm{gw}}$ is the effective diffusivity tensor of water vapour in the gas phase contained within the pore space, $\beta_{swg} = \beta_s(1\text{-}n)\cdot(S_g\,\rho^{gw} + \rho^w S_w)$ and M_α, M_w and $M_g(\boldsymbol{x},t)$ are the molar mass of dry air, liquid water and gas mixture, respectively.

Similarly, the mass balance equation for the dry air is:

$$\begin{aligned} & -n\rho^{g\alpha}\left[\frac{\partial S_w}{\partial t}\right] + \rho^{g\alpha}\left[1 - S_w\right]\mathrm{div}\left(\frac{\partial \mathbf{u}}{\partial t}\right) + n\left[1 - S_w\right]\frac{\partial \rho^{g\alpha}}{\partial t} - \mathrm{div}\left(\rho^g \frac{M_\alpha M_w}{M_g^2} \mathbf{D}_{\mathrm{g}}^{\mathrm{g}\alpha} \mathrm{grad}\left(\frac{p^{g\alpha}}{p^g}\right)\right) \\ & + \mathrm{div}\left(\rho^{g\alpha} \frac{\mathbf{k}^{\mathrm{g}} k^{rg}}{\mu^g}\left[-\mathrm{grad}(p^g) + \rho^g \mathbf{g}\right]\right) - \left[1 - n\right]\beta_s \rho^{g\alpha}\left[1 - S_w\right]\frac{\partial T}{\partial t} = 0 \end{aligned} \tag{3}$$

2.3 Enthalpy balance equation

The enthalpy balance equation of the mixture has the following form:

$$\left(\rho C_p\right)_{eff}\frac{\partial T}{\partial \mathrm{t}}+\rho^w C_p^w\left[\frac{\mathbf{k}^{\mathrm{w}}k^{rw}}{\mu^w}\left[-\mathrm{grad}(p^g)+\mathrm{grad}(p^c)+\rho^w\mathbf{g}\right]\right]\cdot\mathrm{grad}T$$
$$+\rho^g C_p^g\left[\frac{\mathbf{k}^g k^{rg}}{\mu^g}\left[-\mathrm{grad}(p^g)+\rho^g\mathbf{g}\right]\right]\cdot\mathrm{grad}T-\mathrm{div}\left(\chi_{eff}\,\mathrm{grad}T\right)=-\dot{\mathrm{m}}_{\mathrm{vap}}\Delta\mathrm{H}_{\mathrm{vap}} \tag{4}$$

where, $\rho(C_p)_{eff}$ is the effective thermal capacity of the porous medium, $C_p^w(\boldsymbol{x},t)$ and $C_p^g(\boldsymbol{x},t)$ are the specific heat of the water and gas mixture respectively, and $\chi_{eff}(\boldsymbol{x}, t)$ is the effective thermal conductivity of the porous medium. The right hand side term of Eq. (4) considers the contribution of the evaporation and condensation.

2.4 Constitutive equations

To complete the description of the mechanical behaviour, constitutive equations have to be specified. For the gas phase which is assumed to be a perfect mixture of two ideal gases, the state equation of a perfect gas (Clapeyron's equation) and Dalton's law are applied to dry air ($g\alpha$), water vapour (gw) and moist air (g). In the partially saturated zones, the water vapour pressure $p^{gw}(\boldsymbol{x}, t)$ is obtained from the Kelvin-Laplace equation. The saturation $S_\pi(\boldsymbol{x}, t)$ and the relative permeability $k^{r\pi}(\boldsymbol{x},t)$ are experimentally determined functions of the capillary pressure p^c and the temperature T.

The behaviour of the solid skeleton is described within the framework of elasto-viscoplasticity theory for geometrically linear problems. The generalized effective stress state is limited by the Drucker-Prager yield surface with isotropic linear hardening and non-associated plastic flow as a first approximation:

$$f\left(p',\mathbf{s}',\mathrm{q}\right)=3\alpha_f p'+\left\|\mathbf{s}'\right\|-\beta_f\sqrt{\frac{2}{3}}\left[\mathrm{c}_0+\mathrm{H}\xi^{\mathrm{vp}}\right] \tag{5}$$

In Eq. (5) p' = (1/3)tr$\boldsymbol{\sigma}$' is the mean effective Cauchy pressure, $\|\mathbf{s}'\|$ is the norm of the deviator effective Cauchy stress tensor $\boldsymbol{\sigma}'$, c_0 is the apparent cohesion, α_f and β_f are two material parameters related to the friction angle φ of the soil defined by Eq. (6), H is the hardening/softening modulus and ξ^{vp} is the equivalent viscoplastic strain. The flow rule is of non-associated type, with the plastic potential function given by Eq. (5) but with the dilatancy angle ψ substituting the friction angle in Eq. (6).

$$\alpha_f=2\frac{\sqrt{2/3}\sin\varphi}{3-\sin\varphi}\quad,\quad \beta_f=2\frac{6\cos\varphi}{3-\sin\varphi} \tag{6}$$

The viscoplastic constitutive relationships employed to model the soil behaviour are briefly outlined in the following section.

2.5 Viscoplasticity (local and non-local) – A synopsis

The total strain rate in an elasto-viscoplastic material is additively decomposed into an elastic and a viscoplastic strain rate:

$$\dot{\boldsymbol{\varepsilon}} = \dot{\boldsymbol{\varepsilon}}^{\mathrm{e}} + \dot{\boldsymbol{\varepsilon}}^{\mathrm{vp}} \tag{7}$$

where the superimposed dot denotes time derivative. Considering linear elasticity, the stress rate is related to the strain rate via the following constitutive relation:

$$\dot{\boldsymbol{\sigma}} = \mathbf{D}^{\mathrm{e}} : \left(\dot{\boldsymbol{\varepsilon}} - \dot{\boldsymbol{\varepsilon}}^{\mathrm{vp}} \right) \tag{8}$$

where $\mathbf{D}^{\mathrm{e}}$ is the fourth-order elastic tensor and double dots ":" denote the doubly contracted tensor product.

Two commonly used models, the Perzyna model [22] and Duvaut-Lions model [23] belong to this category. The difference between these two models is based on the different choice of the viscoplastic strain rate. Herein the first model will be treated.

In the viscoplastic model proposed by Perzyna (which from this point on will be referred as local to distinguish from non-local), the viscoplastic strain rate is directly linked to the yield function through the viscous nucleus:

$$\dot{\boldsymbol{\varepsilon}}^{\mathrm{vp}} = \gamma \left\langle \Phi\left(\frac{f}{f_0} \right)^{\mathrm{N}} \right\rangle \frac{\partial \mathrm{g}}{\partial \boldsymbol{\sigma}'} \tag{9}$$

with f being the yield function, f_0 introduced as a reference fixed value making the viscous nucleous dimensionless, γ is a "fluidity" parameter which depends on the viscosity η of the material ($\gamma=1/\eta$) and can be constant or a function of the stress or strain rate, N is a calibration parameter ($\mathrm{N} \geq 1$) and g is the viscoplastic potential function. Associative flow is invoked by $\mathrm{g}=f$.

In Eq. (9), "$\langle\cdot\rangle$" are the McCauley brackets, such that:

$$\left\langle \Phi(\mathrm{x}) \right\rangle = \begin{cases} \Phi(\mathrm{x}) & \text{if } \Phi(\mathrm{x}) \geq 0 \\ 0 & \text{if } \Phi(\mathrm{x}) < 0 \end{cases} \tag{10}$$

Non-local approach is introduced next because in case of weakly rate-sensitive materials (such as dense sand) artificial viscosities have to be chosen to obtain objective finite element results. To ensure a regularized numerical solution physically based and following [9], the local viscoplastic model of Perzyna is expanded with respect to another regularization technique, namely the non-local approach.

Briefly speaking, the non-local theory is based on the idea that the response of the material at a point is determined not only by the state at that point but also by the state of its neighbouring points (Fig. 1).

According to Jirásek [24] in non-local approach a certain variable, f, is substituted with its non-local counterpart, $\hat{f}$, obtained by weighted averaging over a spatial neighbourhood (distributing points located at ξ) of each point under consideration (located at x):

$$\hat{f}(\mathrm{x}) = \int_{\mathrm{v}} \alpha(\mathrm{x}, \xi)\, f(\xi) \mathrm{d}\xi \tag{11}$$

Key points for the formulation and implementation of a non-local approach are the chosen weighting function for averaging and as non-locality is introduced into the constitutive equations.

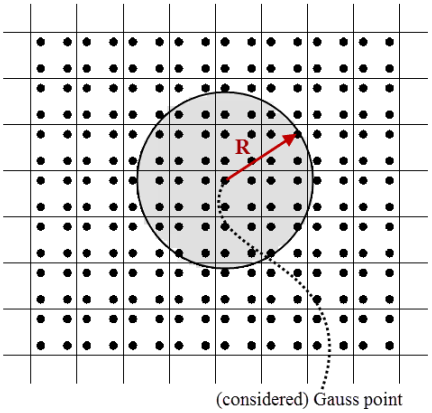

Figure 1: Area where the average is calculated.

The weight function contains at least one parameter with the dimension of length which incorporates information about the microstructure and controls the size of the localized plastic zone [25]. Herein, inspired by [9], the yield function is chosen to be the non-local variable and a Gaussian weighting function with a bounded support is selected (Eq.12 and Fig. 2).

$$\alpha_0(\mathbf{x}-\boldsymbol{\xi}) = \begin{cases} \exp\left(-\dfrac{2\cdot(\mathbf{x}-\boldsymbol{\xi})}{l}\right)^2 & \text{if } \|\mathbf{x}-\boldsymbol{\xi}\| \le R \\ 0 & \text{if } \|\mathbf{x}-\boldsymbol{\xi}\| > R \end{cases} \tag{12}$$

Choosing yield function as the non-local variable, the viscous nucleus and consequently the viscoplastic flow rule are modified:

$$\dot{\boldsymbol{\varepsilon}}^{vp} = \gamma\Phi\left(\hat{f}\right)\frac{\partial g}{\partial \boldsymbol{\sigma}'} \tag{13}$$

The non-local yield function is evaluated using Gauss quadrature [26]:

$$\hat{f}(\mathbf{x}_i) = \frac{\sum_{e=1}^{el}\sum_{j=1}^{n}\omega_j^e\alpha\left(\left\|\mathbf{x}_i-\boldsymbol{\xi}_j^e\right\|\right)\det\mathbf{J}_j^e f(\boldsymbol{\xi}_j^e)}{\sum_{e=1}^{el}\sum_{j=1}^{n}\omega_j^e\alpha\left(\left\|\mathbf{x}_i-\boldsymbol{\xi}_j^e\right\|\right)\det\mathbf{J}_j^e} \tag{14}$$

in which i is the integration point under consideration, j is the jth Gauss point of element e; el is the total number of elements inside the interaction volume defined by a sphere centered at x with radius R (Fig. 1), n is the number of Gauss points of this element inside the interaction volume; ω and $\mathbf{J}$ are, respectively, the weight and Jacobian matrix at Gauss point j of element e.

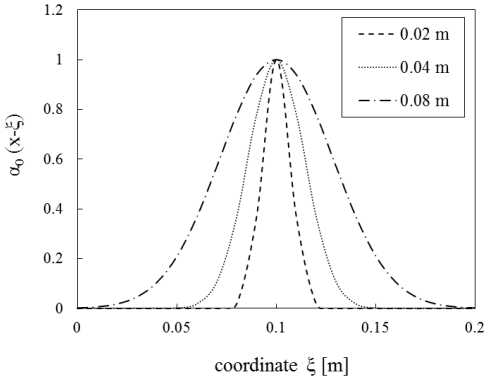

Figure 2: 1-D example of Gaussian weighting function for different values of the internal length scale l (l=0.02, 0.04, 0.08m). The influence of the weighting function increases with increasing values of the internal length scale.

The non-local model is implemented in Comes-geo code in such a manner that the non-local extension to more sophisticated yield criteria is straightforward only by minor modifications in the local model [25]. This feature stems from the fact that the factors $\omega_j^e, \mathbf{J}_j^e, \alpha\left(\left\|\mathbf{x}_i - \boldsymbol{\xi}_j^e\right\|\right)$ of Eq. (14) depend on the finite element mesh itself and not on the material model considered. Therefore, these factors are computed only once at the beginning of the analysis and their values are used in the subsequent iterations, reducing in this way the computational burden. A flowchart of the implementation of the non-local approach is presented in Fig. 3.

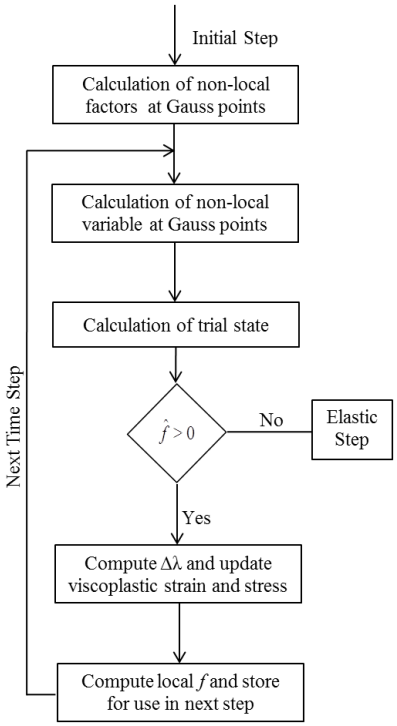

Figure 3: Flowchart of the non-local implementation in Comes-geo code.

3 SLOPE STABILITY TEST

A benchmark slope stability problem, inspired by Regueiro and Borja [28], is now presented to demonstrate the effectiveness of adopting the regularization techniques developed in this work. The dimensions and boundary conditions of the problem are shown in Fig. 4 whereas the soil parameters considered in the analysis are indicated in Table 1. The initial stress field is given by geostatic stress state and as a first approximation fully drained conditions are imposed. Next, a downward displacement with a constant rate of 10^{-3} m/s is applied on a portion of 4m on the top slope surface (Fig. 4). Two meshes with 400 and 1600 eight node quadrilateral isoparametric elements are used to analyze the problem. The analyses are performed using: the elastoplastic model, the local elasto-viscoplastic model of Perzyna with viscosity η=100 s and the non-local elasto-viscoplastic model with an internal length of l=0.8 m. The results from these models are compared in Fig. 5 in terms of equivalent (visco)plastic strain and in Fig. 6 with the force-displacement plots.

Table 1: List of soil parameters for the slope stability problem.

E [MPa]	ν	γ [kN/m^3]	c_0 [kPa]	φ [°]	ψ [°]	h [kPa]	n	k [m^2]
10	0.4	20	40	10	3	-10	0.3	1E-10

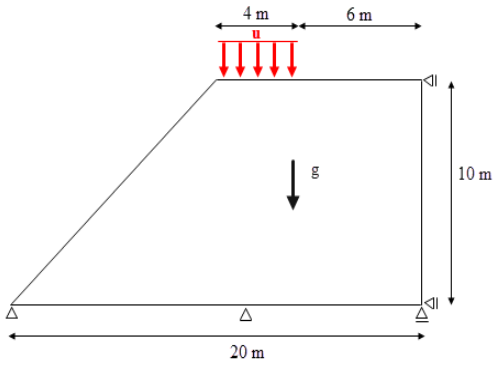

Figure 4: Slope stability problem. Geometry and boundary conditions.

The failure initiates in the element just to the right of the applied force and propagates in a manner depended on the angle of friction. When the elastoplastic constitutive model is used to solve this boundary value problem, a classical mesh dependent numerical solution is observed with the model being unable to simulate the failure process of the slope when the mesh is refined (Fig. 5d). As is shown in Fig. 6b when the elasto-viscoplastic formulation of Perzyna is adopted, even if the number of elements is increased, the shear band formation and the force-displacement relationship are not affected by the element size. However, the peak value of the viscoplastic strain field depends on the element size of the mesh (Fig. 5e). Finally, the non-local elasto-viscoplastic model is able to predict a clearly defined shear band (up to the end of the shear band evolution) and the slope's strain-softening response (Fig. 6c) independently of the mesh adopted (Fig. 5f).

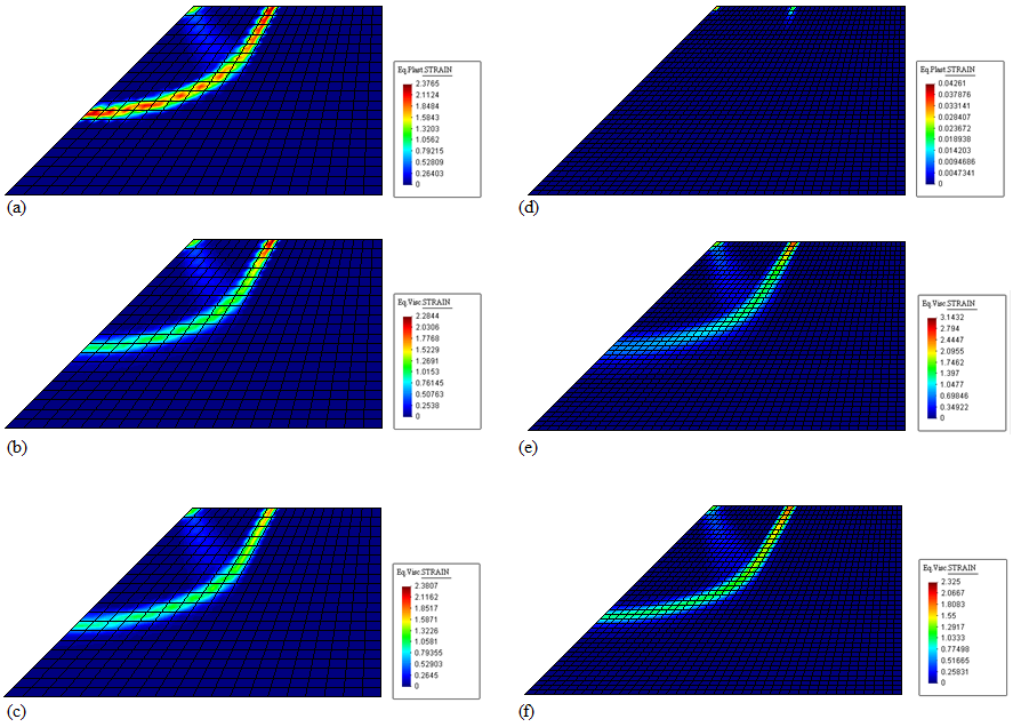

Figure 5: Equivalent (visco)plastic strain contours as calculated using the elastoplastic model (a,d), the local elasto-viscoplastic model (b,e) and the non-local elasto-viscoplastic model (c,f) for a mesh consisting of 400 elements (a), (b) and (c) and for a mesh consisting of 1600 elements (d), (e) and (f), respectively.

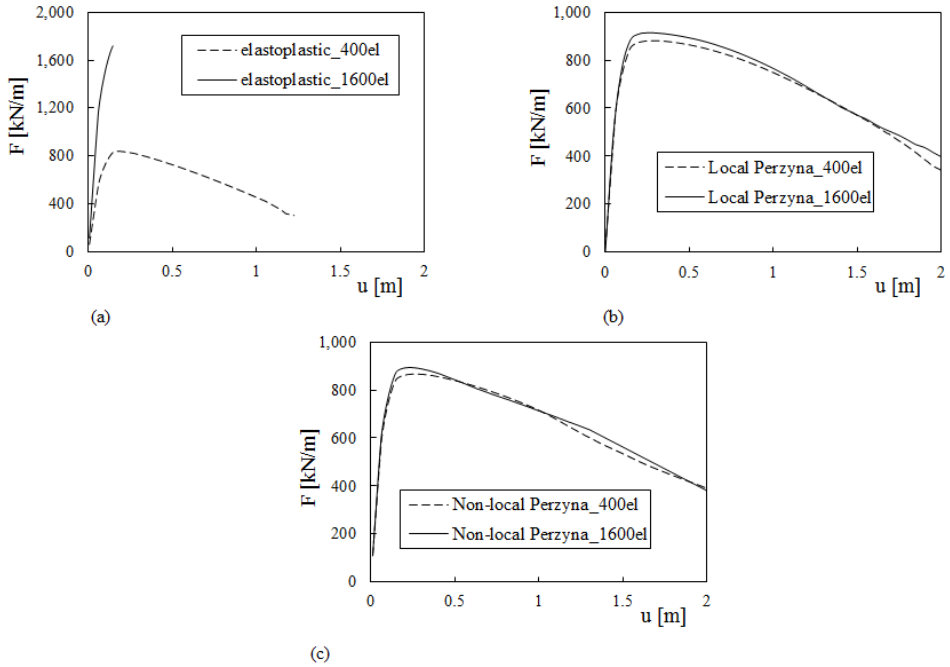

Figure 6: Force-displacement plots for (a) the elastoplastic model, (b) the local elasto-viscoplastic model and (c) the non-local elasto-viscoplastic model, for the two meshes.

4 CONCLUSIONS

In this work the mesh sensitivity problem in strain localization simulation of multiphase geomaterials are overcomed by means of viscoplasticity and nonlocal theories. These formulations are implemented in an existing finite element code for multiphase porous media. Both methods introduce a characteristic length scale (implicitly and explicitly) which prevents strains from localizing into infinitely narrow bands when the mesh is refined. The efficiency of the models in terms of regularized performance is illustrated using a benchmark numerical example of a slope failure problem. The numerical results indicate that only by using the applied regularization techniques the location and the propagation of the shear zone is reliably simulated in a mesh independent manner.

ACKNOWLEDGMENT

The authors would like to thank the 7th Framework Programme of the European Union (ITN MuMoLaDe project 289911) for the financial support of this work.

REFERENCES

[1] Ehlers, W., Graf, T. and Ammann, M. Deformation and localization analysis of partially saturated soil. *Computer Methods in Applied Mechanics and Engineering* (2004) **193**:2885–2910.

[2] Loret, B. and Prevost, J.H. Dynamic strain localization in fluid-saturated porous media. *Journal of Engineering Mechanics* (1991) **117**(4):907-922.

[3] Schrefler, B.A., Zhang, H.W. and Sanavia, L. Fluid-structure interaction in the localization of saturated porous media. ZAMM Zeitschrift für Angewandte Mathematik und Mechanik, *Journal of Applied Mathematics and Mechanics. Z. Angew. Math. Mech.* (1999) **79**:481-484.

[4] Schrefler, B.A, Zhang, H.W and Sanavia, L. Interaction between different internal length scales in fully and partially saturated porous media – The 1-D case, *International Journal for Numerical and Analytical Methods in Geomechanics* (2006) **30**:45-70.

[5] Zhang, H.W and Schrefler, B.A. Gradient-dependent plasticity model and dynamic strain localization analysis of saturated and partially saturated porous media: one dimensional model. *European Journal of Mechanics A/Solids* (2000) **19**(3):503–524.

[6] Ehlers, W. and Volk, W. On theoretical and numerical methods in the theory of porous media based on polar and non-polar elasto-plastic solid materials. *International Journal of Solids and Structures* (1998) **35**:4597-4617.

[7] Lazari, M., Sanavia, L. and Schrefler, B.A. Viscoplastic regularization of strain localization in fluid-saturated porous media. *Proceedings of WCCM XI-ECCM V*, Tomo IV: 3495-3503, Barcelona, (2014). ISBN: 978-84-942844-7-2

[8] di Prisco, C., Imposimato, S. and Aifantis, E.C. A visco-plastic constitutive model for granular soils modified according to non-local and gradient approaches. *International Journal for Numerical and Analytical Methods in Geomechanics* (2002), **26**:121-138.

[9] di Prisco, C. and Imposimato, S. Nonlocal numerical analyses of strain localization in dense sand. *Mathematical and Computer Modelling* (2003) **37**:497-506.

[10] Lewis, R.W. and Schrefler, B.A. *The Finite Element Method in the Static and Dynamic Deformation and Consolidation of Porous Media*, Wiley and Sons: Chichester, (1998).

[11] Schrefler, B.A. Mechanics and thermodynamics of saturated/unsaturated porous materials and quantitative solutions. *Applied Mechanics Reviews* (2002) **55**(4):351-388.
[12] Gray, W.G. and Hassanizadeh, M. Unsaturated flow theory including interfacial phenomena. *Water Resources Research* (1991) **27**:1855-1863.
[13] Hassanizadeh, M and Gray, W.G. General conservation equations for multi-phase system: 1. Averaging technique. *Advances in Water Resources* (1979a) **2**:131-144.
[14] Hassanizadeh, M and Gray, W.G. General conservation Equations for multi-phase system: 2. Mass, momenta, energy and entropy equations. *Advances in Water Resources* (1979b) **2**:191-201.
[15] Hassanizadeh, M. and Gray, W.G. General conservation equations for multi-phase systems: 3. Constitutive theory for porous media flow. Advances in Water Resources (1980) **3**(1):25-40.
[16] Gawin, D. and Schrefler, B.A. Thermo-hydro-mechanical analysis of partially saturated porous materials. *Engineering Computations* (19960 **13**(7):113-143.
[17] Gawin, D. and Sanavia, L. A unified approach to numerical modelling of fully and partially saturated porous materials by considering air dissolved in water. *CMES-Comp. Model. Eng. Sci.* (2009) **53**:255-302.
[18] Gawin, D. and Sanavia, L. Simulation of cavitation in water saturated porous media considering effects of dissolved air. *Transport Porous Media* (2010) **81**:141-160.
[19] Sanavia, L., Pesavento, F. and Schrefler, B.A. Finite element analysis of non-isothermal multiphase geomaterials with application to strain localization simulation. *Computational Mechanics* (2006) **37**:331-348.
[20] Sanavia, L., François, B., Bortolotto, R., Luison, L. and Laloui, L. Finite element modelling of thermo-elasto-plastic water saturated porous materials. *Journal of Theoretical and Applied Mechanics* (2008) **38**:7-24.
[21] Nuth, M. and Laloui, L. Effective stress concept in unsaturated soils: Clarification and validation of a unified approach. *Int. J. Numer. Anal. Methods Geomech.* (2008) **32**:771-801.
[22] Perzyna, P. Fundamental problems in viscoplasticity. *Advances in Applied Mechanics* (1966) **9**:243-377.
[23] Duvaut, G. and Lions, L.J. *Inequalities in Mechanics and Physics*. Springer: Berlin, (1972).
[24] Jirásek, M. Objective modeling of strain localization. *Revue Française de Genie Civil* (2002) **6**:1119-1132.
[25] Jirásek, M. and Rolshoven, S. Comparison of integral-type nonlocal plasticity models for strain-softening materials. *International Journal of Engineering Science* (2003) **41**:1553-1602.
[26] Zienkiewicz, O.C. and Taylor, R.L. *The finite element method*. 5th edition published by Butterworth-Heinemann, (2000).
[27] Lazari, M., Sanavia, L. and Schrefler, B.A. Local and non-local elasto-viscoplasticity in strain localization analysis of multiphase geomaterials. *International Journal for Numerical and Analytical Methods in Geomechanics* (2015), accepted.
[28] Regueiro, R.A. and Borja, R.I. Plane strain finite element analysis of pressure sensitive plasticity with strong discontinuity. *International Journal of Solids and Structures* (2001) **38**:3647-3672.